Fine-structure-changing collision cross sections within the low-lying $n\,^2D$ states of rubidium induced by ground-state rubidium atoms

J. W. Parker, H. A. Schuessler, R. H. Hill, Jr.,* and B. G. Zollars†
Department of Physics, Texas A&M University, College Station, Texas 77843-4242
(Received 11 April 1983)

The thermal cross sections for inelastic transfer of excited rubidium atoms from the $n\,^2D_{5/2}$ to the $n\,^2D_{3/2}$ fine-structure state caused by fine-structure-changing collisions with ground-state rubidium atoms have been measured by selective stepwise excitation of the rubidium atoms and observation of the resulting fluorescence. The cross sections (in units of 10^{-14} cm^2) for n being 5–9 are 2.9±0.6, 6.9±1.4, 11.5±2.3, 17.1±3.0, and 26.0±5.0, respectively. The fine-structure-changing cross sections are of the order of the geometrical cross sections and increase slightly less than $(n^*)^4$ for the low-lying $n\,^2D$ states studied.

I. INTRODUCTION

The application of tunable lasers to the study of excited atomic states has led to a true renaissance of optical techniques in atomic physics. This development is, of course, due to the high spectral power density and ease of tuning of laser-light sources. A particularly active area of research has been the study of inelastic collisions[1,2] between excited atoms and various ground-state atoms. The alkali atoms, with their relatively simple one-electron atomic-core structure, lend themselves to the investigation of collision models allowing experimentally obtained collision cross sections to be compared to calculated values. One class of interesting cross sections is that for collisionally induced transitions between the fine-structure states of the alkali-metal doublets. In such a collision the angular momentum of the excited electron is flipped by the collisional interaction and the electron spin conserves its instantaneous state of motion if the spin is only loosely coupled to the angular momentum. The loose-coupling condition is fulfilled for the states considered since the period of the weak coupling of the angular momentum to the spin is long compared to the duration of the collision. Several experimental[3,4] and theoretical studies[5] of fine-structure-changing collisions in excited alkali-metal states have been reported in recent years and earlier. In two preceding papers[6,7] it was shown that for the $6\,^2D_{5/2}$- and $6\,^2D_{3/2}$- state atoms of rubidum colliding with paramagnetic rubidium ground-state atoms, the fine-structure-changing cross sections are of the order of the geometrical cross sections and that for the diamagnetic noble gases as perturbers, the fine-structure-changing cross sections are about an order of magnitude smaller than the geometrical cross sections. The present work was undertaken to investigate in detail the variation of the fine-structure-changing cross sections as a function of the principal quantum number n for a number of consecutive low and intermediate excited rubidium $n\,^2D$ states. Similar work for cesium $n\,^2D$-state atoms by Tam *et al.*[8] for $n=6$–10 and by Deech *et al.*[9] for $n=8$–14 demonstrated a variation approximately with $(n^*)^4$. Here $n^*=n-\delta$ is the effective quantum number of the excited state and δ is the quantum defect. In contrast, for highly excited Rydberg states, it has been observed[10] that the cross sections eventually decrease as a function of n since the excited atom quickly becomes so large that the "perturber" atom misses the active electron when passing through the excited atom. It has also been shown[11] that the broadening cross sections of optical lines of Rydberg atoms can be interpreted using a simple model and the elastic and inelastic cross sections observed for these states. In addition, an oscillatory behavior of the n dependence of the broadening of the two-photon linewidths by collisions was measured for rubidum and potassium Rydberg states.[12] It is therefore expected that experimental values of fine-structure-changing cross sections for varying principal quantum numbers n also provide a valuable contribution to the interpretation of collision broadening of atoms and of interatomic potential curves computed using extended excited-state wave functions.[13] So far the available fine-structure-changing cross sections for low and intermediate excited ^2D states of rubidium have been obtained by different techniques[3,4,6,10] and are not complete nor consistent enough to make detailed tests of collisional fine-structure mixing possible. With the use of stepwise two-photon excitation the present paper reports new or improved values of fine-structure-changing cross sections for the low-lying rubidium ^2D states with $n=5$–9. The collisions studied may be represented as

$$\mathrm{Rb}(n\,^2D_{5/2})+\mathrm{Rb}(5\,^2S_{1/2}) \underset{\sigma'_{\mathrm{fs}}}{\overset{\sigma_{\mathrm{fs}}}{\rightleftarrows}} \mathrm{Rb}(n\,^2D_{3/2}) + \mathrm{Rb}(5\,^2S_{1/2}) + \Delta E_n \,, \quad (1a)$$

where σ_{fs} and σ'_{fs} are, respectively, the thermal cross sections for the forward and reverse fine-structure-changing collision reactions, and ΔE_n is the energy defect which equals the fine-structure splitting of the $n\,^2D$ doublet. In addition also collisions described by

$$\mathrm{Rb}(n\,^2D_{5/2})+\mathrm{Rb}(5\,^2S_{1/2}) \overset{\sigma_{\mathrm{tr}(5/2)}}{\rightarrow} \mathrm{Rb}(\neq n\,^2D_{5/2} \text{ or } n\,^2D_{3/2}) + \mathrm{Rb}(5\,^2S_{1/2}) + \Delta E' \,, \quad (1b)$$

$$\mathrm{Rb}(n\,^2D_{3/2})+\mathrm{Rb}(5\,^2S_{1/2}) \xrightarrow{\sigma_{\mathrm{tr}(3/2)}} \mathrm{Rb}(\neq n\,^2D_{5/2} \text{ or } n\,^2D_{3/2}) + \mathrm{Rb}(5\,^2S_{1/2}) + \Delta E'' \tag{1c}$$

occur, where the $\sigma_{\mathrm{tr}(5/2)}$ and $\sigma_{\mathrm{tr}(3/2)}$ are the thermal cross sections for collisional transfer out of the doublet, with $\Delta E'$ and $\Delta E''$ being the energy defects of the respective cases.

II. EXPERIMENTAL PROCEDURE

A. Rate equations

Two-photon stepwise excitation of the ground-state rubidium atoms using a radio-frequency (rf) resonance lamp and a cw dye laser selectively populates either the $n\,^2D_{5/2}$ level (which is designated as case 1) or the $n\,^2D_{3/2}$ level (case 2). The two cases are represented schematically in Fig. 1. Two resonant photons of different frequencies are absorbed in sequence during the selective excitation process. A photon from the rf resonance lamp excites the rubidium atom from the $5\,^2S_{1/2}$ ground state to the $5\,^2P_{3/2}$ level, and subsequently a second photon from the cw dye laser excites the atom from the $5\,^2P_{3/2}$ level into one of the $n\,^2D$ states.

The steady-state rate equations that are used to describe the dynamic equilibrium which exists for the population of atoms in the $n\,^2D_{5/2}$ and $n\,^2D_{3/2}$ levels contain source terms representing the transfer of excitation from one of the ^2D levels into the other ^2D level by fine-structure-changing collisions and the direct population of the fine-structure level by laser light, where applicable. Loss terms consist of radiative decay, transfer of atoms out of one of the $n\,^2D$ levels into the other by fine-structure-changing collisions, and transfer of atoms out of the $n\,^2D$ states into various other levels by collisions with ground-state rubidium atoms. Additional gain and loss terms which contribute are treated as generalized gains and losses. The processes contributing to these various terms and their importance are described in the following.

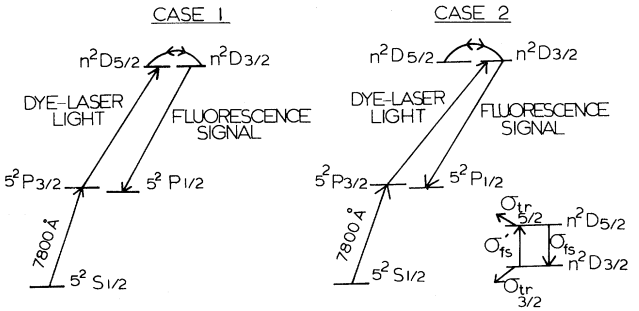

FIG. 1. Partial energy-level diagram showing the rubidium states involved in the two-photon stepwise excitation and emission processes. Case 1 depicts the combined optical and collisional processes which lead to sensitized fluorescence from the $n\,^2D_{3/2}$ state. Case 2 illustrates the direct optical excitation of the $n\,^2D_{3/2}$ state and the resulting fluorescence. In both cases the fluorescence is observed at the same fixed wavelength, which is different from the excitation wavelengths. Various fine-structure-changing cross sections and transfer cross sections are also defined.

For case 1, setting in steady state the production terms equal to the loss terms, the equation for the $n\,^2D_{3/2}$ level population is

$$N^1_{5/2}N\bar{v}\sigma_{\mathrm{fs}}+G^1_{3/2}=N^1_{3/2}[1/\tau_{3/2}+N\bar{v}(\sigma'_{\mathrm{fs}}+\sigma_{\mathrm{tr}(3/2)})] + L^1_{3/2}\ , \tag{2}$$

and for the $n\,^2D_{5/2}$ level population the rate equation is

$$W_{D_{5/2}}+G^1_{5/2}=N^1_{5/2}[1/\tau_{5/2}+N\bar{v}(\sigma_{\mathrm{fs}}+\sigma_{\mathrm{tr}(5/2)})]+L^1_{5/2}\ . \tag{3}$$

For case 2, the steady-state rate equations for the $n\,^2D_{3/2}$ level are

$$W_{D_{3/2}}+G^2_{3/2}=N^2_{3/2}[1/\tau_{3/2}+N\bar{v}(\sigma'_{\mathrm{fs}}+\sigma_{\mathrm{tr}(3/2)})]+L^2_{3/2}\ , \tag{4}$$

and for the $^2D_{5/2}$ level population,

$$N^2_{3/2}N\bar{v}\sigma'_{\mathrm{fs}}+G^2_{5/2}=N_{5/2}[1/\tau_{5/2}+N\bar{v}(\sigma_{\mathrm{fs}}+\sigma_{\mathrm{tr}(5/2)})] + L^2_{5/2}\ . \tag{5}$$

In the rate equations $N_{5/2}$ or $N_{3/2}$ is the number density in the $n\,^2D_{5/2}$ or $n\,^2D_{3/2}$ level and the superscript denotes case 1 or case 2. N is the ground-state rubidium number density, $\bar{v}=(8RT/\pi\mu)^{1/2}$ is the average relative speed of the rubidium atoms, $\tau_{5/2}$ and $\tau_{3/2}$ are the radiative lifetimes, and $W_{D_{5/2}}$ and $W_{D_{3/2}}$ are the production rates of rubidium atoms in the $n\,^2D_{5/2}$ and $n\,^2D_{3/2}$ levels by direct laser excitation from the $5\,^2P_{3/2}$ level. The $G^{1,2}_{5/2,3/2}$ or $L^{1,2}_{5/3,3/2}$ are the generalized gain or loss terms with the superscript denoting case 1 or 2 and the subscript denoting the $n\,^2D_{5/2}$ or $n\,^2D_{3/2}$ state. For instance, in the case of using noble-gas atoms as perturbers as we did in Ref. 7, the gain term contributing on the left-hand side of Eq. (2) is $G^1_{3/2}=N^1_{5/2}N^*\bar{v}^*\sigma^*_{\mathrm{fs}}$, where the "starred" (asterisk superscript) terms represent the parameters with respect to the noble gas. In the present experiment this term could represent the effect of a small amount of contaminant atoms. As another example, consider the gain term consisting of two fine-structure-changing collisions, bringing the atom back to the original state,

$$n\,^2D_{5/2}\xrightarrow{\sigma_{\mathrm{fs}}} n\,^2D_{3/2}\xrightarrow{\sigma'_{\mathrm{fs}}} n\,^2D_{5/2}\ .$$

This process could be considered by an additional gain term on the left-hand side of Eq. (3) as $G^1_{5/2}=N^1_{3/2}N\bar{v}\sigma'_{\mathrm{fs}}$. Equations (2)—(4) can be combined to yield

$$\frac{N^1_{3/2}}{N^2_{3/2}}=\frac{(W_{D_{5/2}}+A)}{(W_{D_{3/2}}+C)}\frac{1}{(1/N\bar{v}\sigma_{\mathrm{fs}}\tau+1+\sigma_{\mathrm{tr}(5/2)}/\sigma_{\mathrm{fs}})} + \frac{B}{(W_{D_{3/2}}+C)}\ , \tag{6}$$

where

$$G^1_{5/2}-L^1_{5/2}=A\ ,\quad G^1_{3/2}-L^1_{3/2}=B\ ,\quad G^2_{3/2}-L^2_{3/2}=C\ .$$

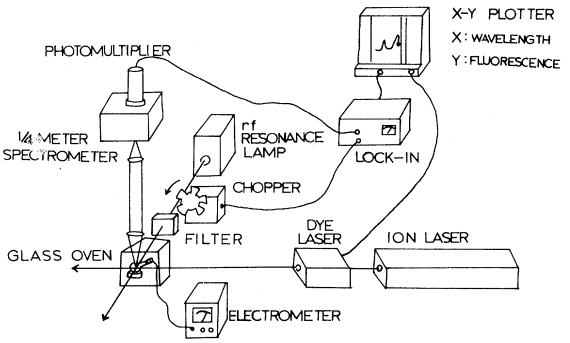

FIG. 2. Schematic diagram of the apparatus.

Equation (6) also gives the ratio of the intensities $I^1_{3/2}/I^2_{3/2}$ of the $n\,^2D_{3/2} \rightarrow 5\,^2P_{1/2}$ sensitized fluorescence of case 1 to the direct fluorescence from the same transition of case 2 as a function of $N\bar{v}$ since the fluorescence intensity from the $n\,^2D_{3/2}$ level is directly proportional to the number density $N_{3/2}$. In specific cases, as in Ref. 7, Eq. (5) can be used to further simplify Eq. (6).

B. Experimental arrangement

Figure 2 depicts the experimental setup. A small glass fluorescence cell containing a few mg of rubidium was located in the center of an electrically heated glass oven. Two different types of cells were used. In the first version, before filling the cell with rubidium and sealing it off, the cell was evacuated and baked for several days at a temperature of 450 °C until a vacuum of better than 10^{-6} Torr was reached. During the experiment the spherical body of the cell (2.5 cm diam) was heated in the oven to a temperature about 50 °C hotter than the temperature of the cell's sidearm (3 cm long, 0.8 cm diam) which contained the rubidium. The sidearm temperature, which was measured with a chromel-alumel thermocouple referenced to an ice bath, determined the rubidium vapor pressure. The second version is shown in Fig. 3. A cylindrical fluorescence cell (4 cm long, 2 cm diam) was connected by a glass capillary (15 cm long, 0.5 mm diam) through a liquid-nitrogen—filled cold trap to a 2.0-l/sec VacIon pump which was turned on permanently. At room temperature the base vacuum in the bulb was better than

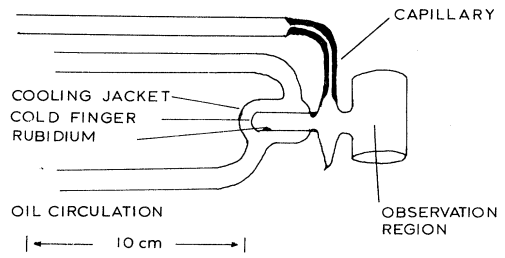

FIG. 3. Picture of the glass resonance cell containing a few mg of rubidium in a temperature-regulated cold finger. The capillary is connected through a liquid-nitrogen—filled cold trap to a VacIon pump.

1×10^{-7} Torr. The cell's cold finger (4 cm long, 0.8 cm diam) had a sealed-on glass jacket through which silicone fluid from a thermostatically controlled bath circulated at various fixed temperatures. During the experiment, at any given temperature setting, the sidearm temperature was held constant to ±0.5 °C and 15—20 °C cooler than the temperature of the body of the fluorescence cell. The cell and cold-finger temperatures were again measured by chromel-alumel thermocouples. The fine-structure-changing cross sections, evaluated from measurements using the two different cells, agree within the experimental errors.

The dye laser (Spectra-Physics 375 without the single-mode etalon and pumped by either an argon-ion or a krypton-ion laser) and the rubidium lamp were arranged horizontally and at 90° angle to each other. The light from the rubidium lamp illuminated the entire volume of the cell with resonant radiation having an intensity of 0.3 mW/cm^2 at 7800 Å. A laser beam with a diameter of approximately 1 cm and an intensity of 100—300 mW/cm^2 passed through the cell along its axis. Experimental parameters for the various $n\,^2D$ states of rubidium are compiled in Table I. The linewidth of the laser, typically between 5 and 20 GHz, was much larger than the Doppler-broadened linewidth of the fluorescence from the $n\,^2D$ states of, typically, 0.5 GHz. Depending on the dye and the dye solvent used, rapid competition between the longitudinal modes (spaced by 400 MHz) of the dye-laser cavity occurs throughout the laser linewidth. To average the mode pattern even more in the case of the $9\,^2D$ state, the output mirror of the dye laser was dithered piezoelectrically at a frequency of a few hundred Hz. The excitation can therefore be considered to be practically "white" as far as each separately excited fine-structure level is concerned.

The fluorescence was observed by a cooled photomultiplier (EMI 9658R, S-20) in the vertical direction through a monochromator (0.25-m Jarrel-Ash) used as a narrow-bandpass filter with a bandpass of about 8 Å. Since the output of the rubidium lamp was modulated at 22.5 Hz with a light chopper, a phase-sensitive lock-in amplifier easily detected the fluorescence signal from the $n\,^2D_{3/2} \rightarrow 5\,^2P_{1/2}$ transition despite the presence of a moderate background of scattered laser light.

C. Data-taking procedure

During a data run the sidearm temperature which determines the rubidium vapor pressure is varied between 105 and 185 °C corresponding to a variation of the rubidium vapor density from 7×10^{12} to 2.4×10^{14} atoms/cm^3. At each temperature setting the dye laser was scanned four or five times across the particular $5\,^2P_{3/2} \rightarrow n\,^2D_{5/2,3/2}$ multiplet of interest (see Table I). The $n\,^2D_{3/2} \rightarrow 5\,^2P_{1/2}$ fluorescence intensity was recorded for each scan as a function of the laser wavelength. The dye-laser and rubidium-lamp intensities were also monitored so that the fluorescence signal could be normalized to constant pumping intensity. Following each temperature increment, typically 3—4 °C, a waiting period of 15—20 min was taken before starting laser scans. This procedure al-

TABLE I. Experimental parameters to study the various $n\,^2D$ states of rubidium. The first excitation step was at the $5\,^2S_{1/2}$-$5\,^2P_{3/2}$ transition at 7800 Å. The dye solvent was in all cases ethylene glycol.

Excitation transition of the second step (cases 1 and 2)	Dye-laser wavelength (Å)	Dye-laser characteristics	Typical dye-laser output (mW)	Observed fluorescence transition	Observed fluorescence wavelength (Å)
$5\,^2P_{3/2}$-$5\,^2D_{5/2}$	7757.6	Oxazine 750 pumped by 5-W red output from a Kr^+ laser	300 (35-GHz bandwidth)	$5\,^2D_{3/2}$-$5\,^2P_{1/2}$	7619.2
$5\,^2P_{3/2}$-$5\,^2D_{3/2}$	7759.7				
$5\,^2P_{3/2}$-$6\,^2D_{5/2}$	6298.3	Rhodamine 101 pumped by 4-W green output from an Ar^+ laser	200 (19-GHz bandwidth)	$6\,^2D_{3/2}$-$5\,^2P_{1/2}$	6206.3
$5\,^2P_{3/2}$-$6\,^2D_{3/2}$	6299.2				
$5\,^2P_{3/2}$-$7\,^2D_{5/2}$	5724.1	Rhodamine 6G pumped by 3-W all-line output from an Ar^+ laser	300 (9-GHz bandwidth)	$7\,^2D_{3/2}$-$5\,^2P_{1/2}$	5647.8
$5\,^2P_{3/2}$-$7\,^2D_{3/2}$	5724.6				
$5\,^2P_{3/2}$-$8\,^2D_{5/2}$	5431.5	Rhodamine 110 pumped by 3-W all-line output from an Ar^+ laser	150 (7-GHz bandwidth)	$8\,^2D_{3/2}$-$5\,^2P_{1/2}$	5362.6
$5\,^2P_{3/2}$-$8\,^2D_{3/2}$	5431.8				
$5\,^2P_{3/2}$-$9\,^2D_{5/2}$	5260.0	Courmarin 6 pumped by 3-W blue output from an Ar^+ laser	100 (5-GHz bandwidth)	$9\,^2D_{3/2}$-$5\,^2P_{1/2}$	5195.3
$5\,^2P_{3/2}$-$9\,^2D_{3/2}$	5260.2				

lowed the fluorescence cell to equilibriate to the new temperature. Our results show no dependence on whether a particular data run started at the upper or lower end of the temperature range.

Figure 4 shows fluorescence signals recorded during single-laser scans at three different temperatures for the rubidium $7\,^2D$ states. The signal peak on the left-hand side (toward the blue end of the spectrum) corresponds to the sensitized fluorescence produced when the $n\,^2D_{3/2}$ level was populated indirectly through fine-structure-changing collisions (case 1). The signal peak on the right-hand side (toward the red) corresponds to direct fluorescence produced when the $n\,^2D_{3/2}$ level was populated directly by the two-photon stepwise excitation (case 2). As $N\bar{v}$ increases with temperature, fine-structure-changing collisions occur more frequently causing the relative yield of sensitized fluorescence to increase compared to direct fluorescence. For each $n\,^2D$ doublet, the ratio of the intensities of the two fluorescence signals was measured at each temperature setting and used to determine the fine-structure-changing cross sections.

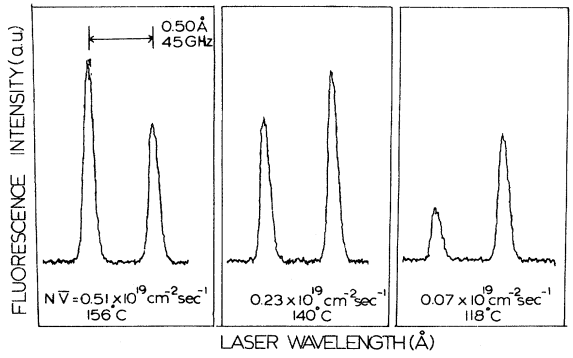

FIG. 4. Fluorescent light intensity from the $7\,^2D_{3/2}$ state to the $5\,^2P_{1/2}$ state at $\lambda = 5647.8$ Å as the laser is tuned from the $7\,^2D_{5/2}$ state (case 1) to the $7\,^2D_{3/2}$ state (case 2) for three different cell temperatures.

III. DATA ANALYSIS AND DISCUSSION

Typical data for the various $n\,^2D$ states of rubidium investigated is compiled in Fig. 5. Before using the expressions of Eq. (6) to extract the fine-structure-changing cross section σ_{fs}, simplifying assumptions must be made. Firstly, the thermal cross sections σ_{fs} and $\sigma_{tr(5/2)}$ are assumed to be independent of temperature over the small range of this experiment. This is corroborated by previous measurements.[4,9] Secondly, we see that Eq. (6) can be further simplified. Since the terms $W_{D_{5/2}}$ and $W_{D_{3/2}}$ are the excitation rates by direct laser excitation, and the terms $A-C$ are small-perturbation terms due to second-order processes, etc., it follows that $W_{D_{5/2}} \gg A$ and $W_{D_{3/2}} \gg C$. It should be noted that each of the terms $A-C$ is comprised of a gain term minus a loss term, and therefore, as the gains into a state tend toward the losses from a state, as, for instance, in energy pooling back and forth, these terms go toward zero. Hence, Eq. (6) can be rewritten as

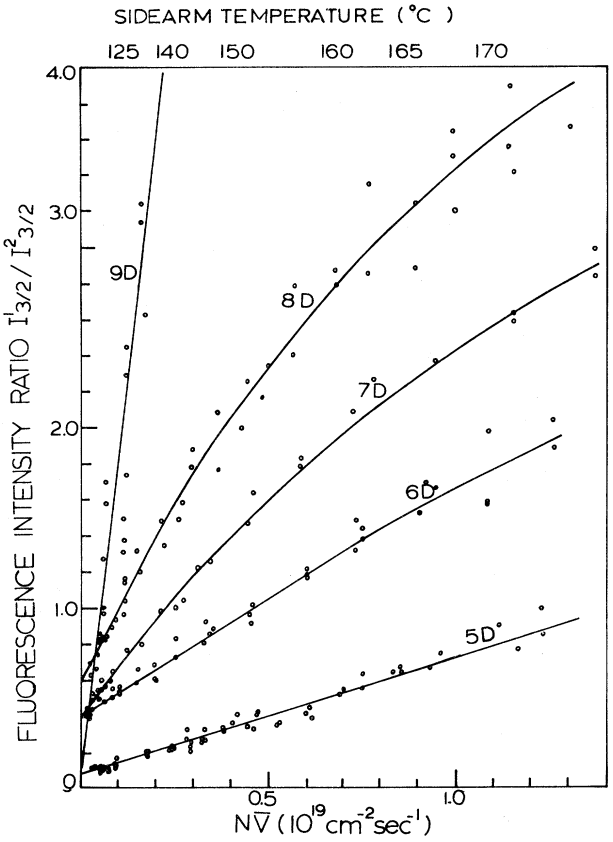

FIG. 5. Compilation of the observed fluorescent light intensity ratio vs $N\bar{v}$ for all the rubidium $n\,D$ states investigated. Sidearm temperatures are also listed on the horizontal axis.

$$\frac{I^1_{3/2}}{I^2_{3/2}}=\frac{f_{P\to D_{5/2}}}{f_{P\to D_{3/2}}}\frac{1}{(1/N\bar{v}\sigma_{fs}\tau_{5/2}+1+\sigma_{tr(5/2)}/\sigma_{fs})}+Q\,, \tag{7}$$

where $Q=B/(W_{D_{3/2}}+C)\approx B/W_{D_{3/2}}$. It was also considered that for constant-rf lamp and dye-laser excitations, the production rates are related to the oscillator strengths $f_{P\to D}$ by

$$W_{D_{5/2}}/W_{D_{3/2}}=f_{P\to D_{5/2}}/f_{P\to D_{3/2}}\,. \tag{8}$$

The oscillator strengths are derived from the Einstein coefficients which are calculated with a procedure outlined previously.[14] In the calculation the radial elements cancel in the ratio and only the angular-momentum terms contribute. The value obtained is $f_{P\to D_{5/2}}/f_{P\to D_{3/2}}=9.00$.

For each data run the values of $\sigma_{fs}\tau_{5/2}$, $\sigma_{tr(5/2)}/\sigma_{fs}$, and Q are determined by fitting the intensity ratios as a function of $N\bar{v}$. The fitted curves are also displayed in Fig. 5. One can see that for low values of $N\bar{v}$ near the origin, the fluorescence intensity ratio follows a straight line of slope $9.00\sigma_{fs}\tau_{5/2}$ and intercept Q. For the different states investigated, that is to say as a function of n, the slope of the curves at low $N\bar{v}$ becomes progressively steeper since both the cross sections and lifetimes are increasing. Since the intercept $Q=B/(W_{D_{3/2}}+C)$ depends on both gain and loss terms as well as the direct laser-excitation term $W_{D_{3/2}}$, no simple significance can be put on its progression as a function of n, since as n progresses, different nearby level structures occur in the rubidium atom and also different dye and laser configurations (hence bandwidths) have been used (see Table I).

A number of collisional processes contribute to the generalized gain and loss terms A—C. These processes include collisions with atoms in excited rubidium P states which are important at high rubidium densities due to radiation trapping, wall collisions which are important at low rubidium densities N, energy pooling back and forth between other nearby states due to angular-momentum mixing, collisions with molecular Rb_2 which is present in the resonance cell, collisions with trace amounts of other gases (such as cesium which is a naturally occurring impurity in rubidium), photoionization by a second-laser photon in a three-step process or photoionization from the glass windows and subsequent collisions with the photoelectrons, three-body collisions involving the excited-state atom and two other atoms, and associative ionization and subsequent recombination.

Care was taken to perform the measurements under conditions where all these effects are minimal and small against the measurement uncertainties. A low rubidium-atom density of about $N=7\times10^{12}$—2.4×10^{14} cm^{-3} was used. At the highest operating temperature (185 °C) of the resonance cell the molecular Rb_2 density is 3 orders of magnitude lower than the atomic density. Photoionization by the unfocused mW cw laser is also negligible.

One additional process that has recently received much attention is that of the background black-body radiation[15] inducing transitions to nearby resonant states. For instance, in collision experiments in which small background signals were observed and at first attributed to collisions between Rydberg atoms and residual gas atoms, it was later shown[16] that the signals were the result of photoexcitation and photoionization of the Rydberg atoms by room-temperature background radiation. In pulsed experiments this effect can even lead to superradiant cascading[17] and maser action.[18] In deriving Eq. (8) we have denoted $\tau_{5/2}$ to be the radiative lifetime of the $n\,^2D_{5/2}$ state. However, since $T\neq0$ in the present experiment, the background black-body radiation will also cause transitions through stimulated emission from the $n\,^2D_{5/2}$ state,

TABLE II. Compilation of experimental and theoretical lifetimes. All values in nsec.

n	Experimental		Theoretical
5	230±23[a]		266.2[d]
6	237±15[a]	285±16[b]	295.0[d]
7	325±22[a]	388±25[b]	386.0[d]
8	421±25[a]	515±30[b]	532.0[d]
9	568±35[a]	565±120[c]	722.0[d]

[a]Reference 19.
[b]Reference 20.
[c]Reference 21.
[d]Reference 22.

absorption from the $n\,^2D_{5/2}$ state, and finally absorption from nearby states into the $n\,^2D_{5/2}$ state. Table II shows a compilation of recent experimental measurements of the lifetimes of interest[19–21] as well as one set of theoretically calculated lifetimes using a numerical Coulomb approximation.[22] One can see that the experimental values are generally smaller than those of the theoretical calculation. This can be partially resolved by taking the background black-body radiation[21] effects into account yielding the experimental decay rate

$$\frac{1}{\tau_{\text{expt}}}=\frac{1}{\tau_{\text{sp}}}+\frac{1}{\tau_{\text{BB}}}\ , \tag{9}$$

where τ_{expt} is the experimentally measured lifetime, τ_{sp} is the spontaneous emission lifetime and τ_{BB} is the contribution from the background black-body terms. To get an estimate of how important these terms are in the present experiment, the ratio $(1/\tau_{\text{BB}})/(1/\tau_{\text{sp}})$ is considered. In the present experiment, the absorption from other nearby states into the $n\,^2D_{5/2}$ will make only a minor contribution compared to the stimulated emission and absorption from the $n\,^2D_{5/2}$ state and will be neglected. For highly excited Rydberg states, Cooke and Gallagher[15] have used the oscillator-strength sum rule to obtain an approximate formula for the black-body contribution in hydrogenlike atoms. However, the present experiment is in the intermediate region ($n=5$–9 or $n^*=3.7$–7.7) and explicit summations were carried out to obtain the results. The mean photon number[23] $\bar{n}_\omega$ for black-body radiation is

$$\bar{n}_\omega=1/(e^{\hbar\omega/kT}-1)\ , \tag{10}$$

where $\hbar$ is Planck's constant, k is Boltzmann's constant, T is the absolute temperature, and ω is the photon frequency. With the use of the relationships among the Einstein coefficients, the following equation for state j (equal to $n\,^2D_{5/2}$ in this experiment) is obtained:

$$1/\tau_{\text{BB}}=\sum_{\substack{j'\\ E_j>E_{j'}}} A_{jj'}\bar{n}_\omega+\sum_{\substack{j'\\ E_{j'}>E_j}} A_{j'j}(g_{j'}/g_j)\bar{n}_\omega\ , \tag{11}$$

where the first summation represents stimulated emission and the second summation represents absorption, with $E_{j',j}$ being the energy of state j', and j and $g_{j',j}$ the degeneracy factor of state j' and j, respectively. Using the energy levels of Moore[24] and the Einstein coefficients $A_{jj'}$ (spontaneous emission) of Lingard and Nielsen[22] and terminating the summations when no further significant contribution is being added, one finds that for the $9\,^2D_{5/2}$ state the ratio $(1/\tau_{\text{BB}})/(1/\tau_{\text{sp}})$ is less than 0.12. The background black-body contributions become increasingly less important for lower principal quantum numbers n, since the energy spacings become larger until for $n=5$ the ratio is less than 0.01.

Therefore, based on the above considerations, it was concluded that for the present experiment the best approach to account for black-body–radiation effects is to use the experimentally measured lifetimes which already include the effects of the background black-body radiation. In Eq. (7) the radiative lifetime $\tau_{5/2}$ is then considered to include all radiative contributions and, for the present analysis, the experimental values of Marek and Münster[19] were used. Since the parameter of importance from Eq. (7) is $\sigma_{\text{fs}}\tau_{5/2}$, the modification of the results using better lifetime values when they become available can easily be computed.

The measured values of σ_{fs} are listed in Table III along with measurements by Wolnikowski *et al.*[3] for the $7\,^2D$ states, Glodz *et al.*[4] for the $8\,^2D$ state, and Gounand *et al.*[25] for the $9\,^2D$ state. The uncertainty of approximately 20% of the cross sections σ_{fs} and σ'_{fs} is obtained by adding in quadrature the statistical uncertainty in the fitted value of the cross sections (typically 10%), the uncertainty in the radiative lifetime (about 5%), the uncertainty in the determination of $N\bar{v}$ (15%) due to the combined uncertainty in measuring the cold-finger temperature, and the uncertainties in the temperature–to–vapor-pressure conversion formula given by Nesmeyanov.[26] The present experiment was carried out at low temperatures and the value $N\bar{v}(1+\sigma_{\text{tr}(5/2)}/\sigma_{\text{fs}})$ never became large compared to that of $1/\tau_{5/2}\sigma_{\text{fs}}$. Therefore, the transfer cross sections

TABLE III. Compilation of experimental cross sections for fine-structure-changing collisions σ_{fs} and σ'_{fs} in the low-lying $n\,^2D$ states of rubidium. Corresponding geometrical cross sections σ_{geom} were calculated for comparison. All cross-sectional values are in units of 10^{-14} cm^2. The fine-structure splittings ΔE are also listed.

n	σ_{fs} ($n\,D_{5/2}\rightarrow n\,D_{3/2}$)		σ'_{fs} ($n\,D_{3/2}\rightarrow n\,D_{5/2}$)		σ_{geom} n^*		ΔE (cm^{-1})
5	2.9±0.6[a]		4.4±0.9[a,f]		4.9	3.71	2.96
6	6.9±1.4[a]	7.4±2.5[b]	10.4±2.1[a,f]	11.1±3.8[b,f]	11.7	4.68	2.26
7	11.5±2.3[a]	18.0±3.0[c]	17.3±3.5[a,f]	30.0±5.0[c]	24.4	5.67	1.51
8	17.1±3.0[a]	55±11[d]	25.7±4.5[a,f]	81.5±16[d]	45.6	6.66	1.01
9	26.0±5.0[a]	46±15[e]	39.0±7.5[a,f]	70.3±30[e]	78.9	7.66	0.70

[a]This work.
[b]Reference 7.
[c]Reference 3.
[d]Reference 4.
[e]Reference 25.
[f]Calculated using the principle of detailed balancing $\sigma_{\text{fs}}/\sigma'_{\text{fs}}=\exp(\Delta E/kT)g(^2D_{3/2})/g(^2D_{5/2})$, which predicts $\sigma'_{\text{fs}}=1.5\sigma_{\text{fs}}$. Hereby it was used that $\Delta E\ll kT$ and that the statistical weights are $g(^2D_{3/2})=4$ and $g(^2D_{5/2})=6$.

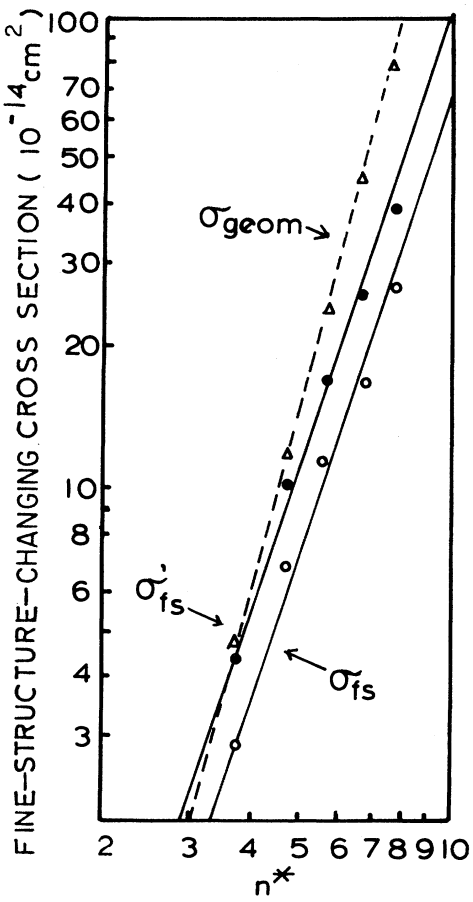

FIG. 6. Plot of the fine-structure-changing cross sections σ_{fs} and σ'_{fs} vs the effective quantum number n^*. Calculated geometrical cross sections σ_{geom} are also indicated.

$\sigma_{tr(5/2)}$ cannot be evaluated without a large statistical uncertainty and are, for that reason, not included in Table III. It can be seen that the values of σ_{fs} found in other experiments are generally larger than the ones determined in the present experiment. This is particularly apparent for the high-n states investigated, where some of the previous values are found to be nearly twice as large. In our view the reason for this may be a compilation of systematic effects which are difficult to take into account when pulsed-laser—excitation schemes are employed, as was done in all the experiments yielding higher values. It has been pointed out recently[27] that in pulsed experiments contamination by photoionization-produced dimer ions will be more severe than in cw experiments. In addition the pulsed two-photon—excitation[3,4] and even the pulsed stepwise-excitation[25] schemes require laser intensities where photoionization from the excited atomic state by a three-step process could be more important than for the low-power cw-excitation scheme used here. Also repopulation and stimulated-emission processes though small are not always negligible in particular for the higher-n states where several closeby neighboring fine-structure states exist.

In our experiment using a broad-band cw laser of low spectral power density (see Table I), the ratio of the observed fluorescent light intensities did not vary when the rubidium lamp and/or the laser intensities were changed. Repopulation and stimulated-emission effects were taken into account or estimated to be negligible. The use of measured rather than calculated lifetimes considers to a

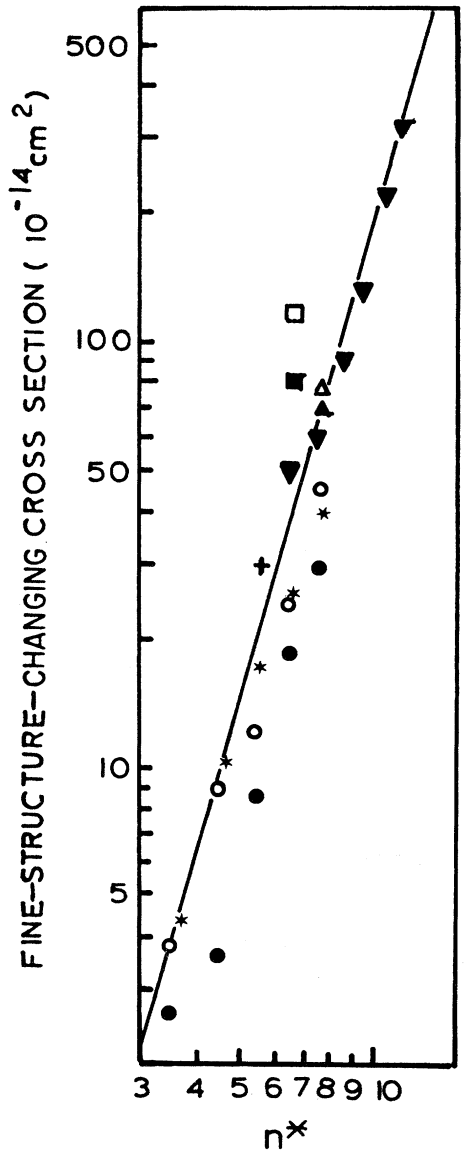

FIG. 7. Compilation of measured fine-structure-changing cross sections σ'_{fs} for low-lying ^2D states of rubidium and cesium vs the effective quantum number n^*. Results obtained in different laboratories by different methods are listed. The notation is *—σ'_{fs} (Rb), this work; +—σ'_{fs} (Rb), Ref. 3; ■—σ'_{fs} (Rb), Ref. 4; □—$\sigma'_{fs}+\sigma_{tr(3/2)}$ (Rb), Ref. 4; ▲—σ'_{ds} (Rb) Ref. 25; △—$\sigma'_{fs}+\sigma_{tr(3/2)}$ (Rb), Ref. 25; ●—$\sigma'_{fs}+\sigma_{tr(3/2)}$ (Cs), Ref. 8; ○—$\sigma_{fs}+\sigma_{tr(3/2)}$ (Cs), Ref. 8; and ▼—$\sigma'_{fs}+\sigma_{tr(3/2)}$ (Cs), Ref. 9. For comparison the calculated geometrical cross section σ_{geom} for rubidium atoms in the $n\,^2D$ state is shown by the solid line.

major part the effects of black-body radiation. In addition extreme care of using pure-rubidium vapor in a high-vacuum cell was applied.

In the absence of rigorous theoretical calculations of fine-structure-changing cross sections for the low-lying $n\,^2D$ state of the alkali-metal atoms, more insight into the collision process is provided by comparing the measured fine-structure-changing cross section with the geometrical cross sections which can be calculated from the hydrogenic expectation values. This gives

$$\sigma_{\text{geom}}=\pi\langle r_n+r_g\rangle^2=\pi(\langle r_n^2\rangle+2\langle r_g\rangle+\langle r_g^2\rangle)\,, \qquad (12)$$

where $\langle r_n^2\rangle$ and $\langle r_g^2\rangle$, the mean radii of the excited-state and ground-state Rb atoms, are given by[28]

$$\langle r^2\rangle=\tfrac{1}{2}n^{*2}[5n^{*2}+1-3l(l+1)]a_0^2\,, \qquad (13)$$

and $\langle r_n\rangle$ and $\langle r_g\rangle$, the mean-square radii, are given by

$$\langle r\rangle=n^{*2}\{1+\tfrac{1}{2}[1-l(l+1)/n^{*2}]\}a_0\,. \qquad (14)$$

Here a_0 is the Bohr radius and l is the orbital angular-momentum quantum number. Figure 6 displays the magnitude and n^* dependence of the various measured and calculated cross sections. It can be seen that in the low-n region the magnitudes of the fine-structure-changing cross sections σ_{fs} and σ'_{fs} are described relatively well by σ_{geom}. However, the geometrical cross section increases faster with n^* than the measured values of σ_{fs} and σ'_{fs} which is more apparent at the higher-n^* values where the $n\,D$ states are closer to resonance with neighboring states of different angular momentum. A compilation of the experimental values of σ'_{fs} for the various low-lying alkali-metal atom ^2D states is shown in Fig. 7 for rubidium and cesium $n\,^2D$ atoms. The values for the cross section $\sigma'_{\text{fs}}+\sigma_{\text{tr}(3/2)}$, which in Ref. 9 is called the depopulation cross section, are also listed. Again σ_{geom} for rubidium atoms is shown by the solid line. This graph suggests that for the intermediate excited-state alkali-metal atoms the $n\,^2D$ fine-structure-changing cross sections scale approximately as the geometric cross section. It is clear that the low-n and intermediate-n regions of the $n\,D$ states of rubidium, where the atom has a tightly bound active electron with a rather extended wave function, require a detailed theoretical investigation, and it is hoped that the present work will stimulate renewed interest in theoretical work in this area.

ACKNOWLEDGMENTS

This research was supported by the National Science Foundation under Grant No. PHY-81-11943 and by the Center for Energy and Mineral Resources at Texas A&M University.

*Present address: U.S. Air Force Weapons Laboratory, Kirtland Air Force Base, Albuquerque, NM 87117.

†Present address: Department of Physics, Rice University, Houston, TX 77001.

[1]For a review see, for example, M. Ebel, in *Progress in Atomic Spectroscopy,* edited by W. Hanle and H. Kleinpoppen (Plenum, New York, 1979), p. 1299.

[2]L. Krause, Appl. Opt. 5, 1375 (1966).

[3]J. Wolnikowski, J. B. Atkinson, J. Supronowicz, and L. Krause, Phys. Rev. A 25, 2622 (1982).

[4]M. Glodz, J. B. Atkinson, and L. Krause, Can. J. Phys. 59, 548 (1981).

[5]E. de Prunele and J. Pascale, J. Phys. B 12, 2511 (1979).

[6]R. H. Hill, Jr., H. A. Schuessler, and B. G. Zollars, Phys. Rev. A 25, 834 (1982).

[7]B. G. Zollars, H. A. Schuessler, J. W. Parker, and R. H. Hill, Jr., Phys. Rev. A 27, (1983).

[8]A. C. Tam, T. Yabuzaki, S. M. Curry, M. Hou, and W. Happer, Phys. Rev. A 17, 1862 (1978).

[9]J. S. Deech, R. Luypaert, L. R. Pendrill, and G. W. Series, J. Phys. B 10, L137 (1977).

[10]M. Hugon, F. Gounand, P. R. Fournier, and J. Berlande, J. Phys. B 12, 2707 (1979); M. Hugon, F. Gounand, P. R. Fournier, and J. Berlande, *ibid.* 13, 1585 (1980).

[11]F. Gounand, J. Szudy, M. Hugon, B. Sayer, and P. R. Fournier, Phys. Rev. A 26, 831 (1982).

[12]B. P. Stoicheff, in *Laser Spectroscopy,* edited by A. R. W. McKellar, T. Oka, and B. P. Stoicheff (Springer, Berlin, 1982), p. 299; B. P. Stoicheff and E. Weinberger, Phys. Rev. Lett. 44, 733 (1980).

[13]J. Pascale and J. Vandeplanque, J. Chem. Phys. 60, 2278 (1974).

[14]O. S. Heavens, J. Opt. Soc. Am. 51, 1058 (1961).

[15]T. F. Gallagher and W. E. Cooke, Phys. Rev. Lett. 42, 385 (1979); W. E. Cooke and T. F. Gallagher, Phys. Rev. A 21, 588 (1980).

[16]E. J. Beiting, G. F. Hildebrant, F. G. Kellert, G. W. Foltz, K. A. Smith, F. B. Dunning, and R. F. Stebbings, J. Chem. Phys. 70, 3551 (1979); G. F. Hildebrant, E. F. Beiting, C. Higgs, G. J. Hatton, K. A. Smith, F. B. Dunning, and R. F. Stebbings, Phys. Rev. A 23, 2978 (1981).

[17]F. Gounand, M. Hugon, P. R. Fournier, and J. Berlande, J. Phys. B 12, 547 (1979).

[18]M. Gross , P. Goy, C. Fabre, S. Haroche, and J. M. Raimond, Phys. Rev. Lett. 43, 343 (1979).

[19]J. Marek and P. Münster, J. Phys. B 13, 1731 (1980).

[20]H. Lundberg and S. Svanberg, Phys. Lett. 56A, 31 (1976).

[21]F. Gounand, M. Hugon, and P. R. Fournier, J. Phys. (Paris) 41, 119 (1980).

[22]A. Lingard and S. E. Nielsen, At. Data Nucl. Data Tables 19, 533 (1977).

[23]R. Loudon, *The Quantum Theory of Light* (Clarendon, Oxford, 1973).

[24]C. E. Moore, in *Atomic Energy Levels,* National Bureau of Standards Circular No. 467 (U.S. G.P.O., Washington, D. C., 1971), Vol. II.

[25]F. Gounand, P. R. Fournier, and M. Hugon, in *Abstracts of Contributed Papers, XIth International Conference on the Physics of Electronic and Atomic Collisions,* edited by K. Takayanagi and N. Oda (The Society for Atomic Collision Research, Tokyo, Japan, 1979).

[26]A. N. Nesmeyanov, *Vapor Pressures of the Elements* (Academic, New York, 1963).

[27]M. Allegrini, W. P. Garver, V. S. Kushawaha, and J. J. Leventhal, Phys. Rev. A 28, 199 (1983).

[28]H. Bethe and E. E. Salpeter, *Quantum Mechanics of One and Two Electron Atoms* (Plenum, New York, 1977).